Detection of the type of intermittency using characteristic patterns in recurrence plots

Katarzyna Klimaszewska and Jan J. Żebrowski
Physics of Complex Systems, Faculty of Physics, Warsaw University of Technology, ulica Koszykowa 75, 00-662 Warszawa, Poland
(Received 26 June 2007; revised manuscript received 18 May 2009; published 25 August 2009)

One of the common routes to chaos is intermittency. Identification of the intermittency type is usually made using the properties of the probability distribution of laminar phases and of the average length of the laminar phases. Both have a statistical character and to obtain them a long time series has to be examined. Here, we present a recurrence plot method applicable to the analysis of short time series and through which the type of intermittency may be identified. The three types of intermittency introduced by Pomeau and Manneville and a chaos-chaos intermittency induced by interior crisis were examined. The identification of the type of intermittency is equivalent to the identification of the bifurcation associated with it. Our result seems particularly interesting as our method allows the analysis of short time series. The effect of the measurement noise on the effectiveness of the method is also discussed. An application of the method to the detection of type I intermittency in measured heart rate variability data is discussed.

DOI: 10.1103/PhysRevE.80.026214 PACS number(s): 05.45.Tp, 89.75.Kd, 82.40.Bj

I. INTRODUCTION

One of the common routes to chaos is intermittency [1]. In such a state, the dynamical system switches between two different kinds of behavior (called phases). The residence time in each of them is different and varies with the time, so that it is impossible to foresee the moment for the next switching. There exist several different types of intermittency (three types of intermittencies investigated by Pomeau and Manneville [2,3], type X [4], V [5,6], and a group of chaos-chaos intermittencies [1] among them the on-off [7] and the in-out [8,9] intermittencies). Each type of the phenomenon is related to a different kind of bifurcation. For example, type I intermittency occurs when the system is close to a saddle-node bifurcation, type II is due to the Hopf bifurcation, and type III—the reverse period doubling bifurcation. One kind of chaos-chaos intermittency is due to crisis phenomena occurring in the system [1]. Thus, the recognition of the type of the intermittency observed in the dynamical system is equivalent to determining the type of the bifurcation characteristic for the dynamics of that system in the particular part of parameter space investigated.

The identification of the intermittency type is usually based on the probability distribution of the length l of the laminar phases—$P(l)$ and the properties of the average length of the laminar phases—$\langle l \rangle$. Both properties have a statistical character. Thus, to obtain them a long time series has to be examined. In practice, often, the length of the time series is limited, so it is important to find a method capable to recognize the type of the intermittency using short time series.

In 2002 Marwan *et al.* [10] showed that it is possible to distinguish between time series with intermittency and with other kinds of chaos using recurrence plots (RP) and recurrence quantification analysis (RQA). They showed that the laminar phases of intermittency correspond to horizontal (and vertical) lines on the RP and that such lines form squares and rectangles [11]. Occurrences of such patterns on the RP are a sign that intermittency is present in the data. However, Marwan *et al.* [10,11] did not define which kind of intermittency they had observed.

It is the aim of this paper to examine the possibility to distinguish the kind of intermittency occurring in the system given the pattern obtained in a recurrence plot and using RQA. We examined four kinds of intermittency: the three types of intermittency defined by Pomeau and Manneville and the chaos-chaos intermittency induced by an interior crisis. To distinguish between the different kinds of intermittency, we extended the RQA of Refs. [10,12] by introducing two parameters. With our method, we were able to determine the type of intermittency even in the presence of a moderately high level of measurement noise.

II. METHOD

A. Recurrence plots and standard quantitative analysis

Recurrence plots were introduced in 1987 by Eckmann *et al.* [13] as a simple, graphical method, useful for examining short time series. The method is based on the Takens embedding theorem [14], which allows reconstructing the phase space of a multidimensional dynamical system from a single observable of the system.

To reconstruct the phase space of the dynamical system studied from a single time series analyzed,

$$X = \{x_1, x_2, \ldots, x_i, \ldots, x_n\}, \tag{1}$$

where n is the length of the series, a time series of $N = n - (m-1)\tau$ vectors,

$$Y = \{\vec{y}_1, \vec{y}_2, \ldots, \vec{y}_i, \ldots, \vec{y}_n\}, \tag{2}$$

has to be prepared with

$$\vec{y}_i = [x_i, x_{i+1}, \ldots, x_{i+(m-1)\tau}], \tag{3}$$

where m is the dimension of the reconstructed phase space (the embedding dimension) and τ is the time delay parameter. The two parameters can be obtained with the use of several algorithms [1,3,15]. In 1987 Albano *et al.* [16] showed that the Takens embedding theorem can be applied also for short time series.

The parameter τ is chosen so that the two scalars from the time series, x_i and $x_{i+\tau}$, may be considered independent.

Here, to obtain τ we calculated the first minimum of the mutual information function (MIF) [17] using the algorithm introduced by Cellucci *et al.* [18], choosing it because of its speed.

The second parameter, which is crucial in constructing the vectors [Eq. (3)], is the embedding dimension—m. To find the best value of m, we used the percentage of false nearest neighbors algorithm [19] implemented in the program Visual Recurrence Analysis (VRA) [20].

Unless otherwise stated in the text or in a figure caption, the recurrence plots presented in this paper were generated with the parameter $m=1$, $\tau=1$ and the cutoff parameter $\epsilon=0.1$.

A recurrence plot is a $N\times N$ matrix M_{ij} calculated from the equation

$$M_{ij}=\Theta(\epsilon-\|\vec{y}_i-\vec{y}_j\|),\quad i,j=1,2,\ldots,N, \tag{4}$$

where Θ is the Heaviside function, and ϵ is a threshold parameter, the value of which is chosen arbitrarily. In our work, we set ϵ equal to 10% of the diameter of the attractor—following Ref. [10]. The matrix M_{ij} is represented graphically as a square composed of $N\times N$ black and white points: black for $M_{ij}=1$ and white when $M_{ij}=0$.

Different behavior of the dynamical system creates different recurrence patterns: long lines parallel to the main diagonal of the RP [Fig. 1(a)] are due to periodic orbits, white noise fills the RP with homogeneously distributed black points [Fig. 1(c)]. For the chaotic state, in a recurrence plot shown in low magnification [Fig. 1(b)] black points on the RP are seemingly uniformly distributed. However, under a larger magnification a distinct pattern of short parallel lines appears and allows us to distinguish between a deterministic chaotic state and random noise [13].

To describe the patterns which occur in an RP, Zbilut *et al.* [12] proposed the RQA. In this analysis the following statistics can be defined on the RP: recurrence (REC)—the percentage of the black points in the RP; determinism (DET)—the percentage of the black points forming lines parallel to the main diagonal of the RP; L_{max}—the maximum length of such lines and Shannon entropy (ENT) of the distribution of these lines. In 2002 Marwan *et al.* [10] showed that, when intermittency occurs in the dynamical system, horizontal and vertical lines are obtained in the RP. These lines correspond to the laminar phases. To describe such lines they added three statistics to RQA: laminarity (LAM)—the percentage of the black points forming vertical lines, trapping time (TT)—the average length of such lines, and V_{max}—the maximum length of the vertical lines. They also noted in Ref. [11] that the horizontal and vertical lines, which are due to the laminar phases, form squares and rectangles.

In this paper, we show that the occurrence of different kinds of intermittency results in various characteristic shapes in the RP pattern—squares or rectangles or distorted squares and rectangles. These shapes allow us to distinguish unambiguously between the different types of intermittency. We supplemented the standard RQA by introducing two parameters F_a and F_b—measures of the surface of area of the regions of the RP representing the laminar phases.

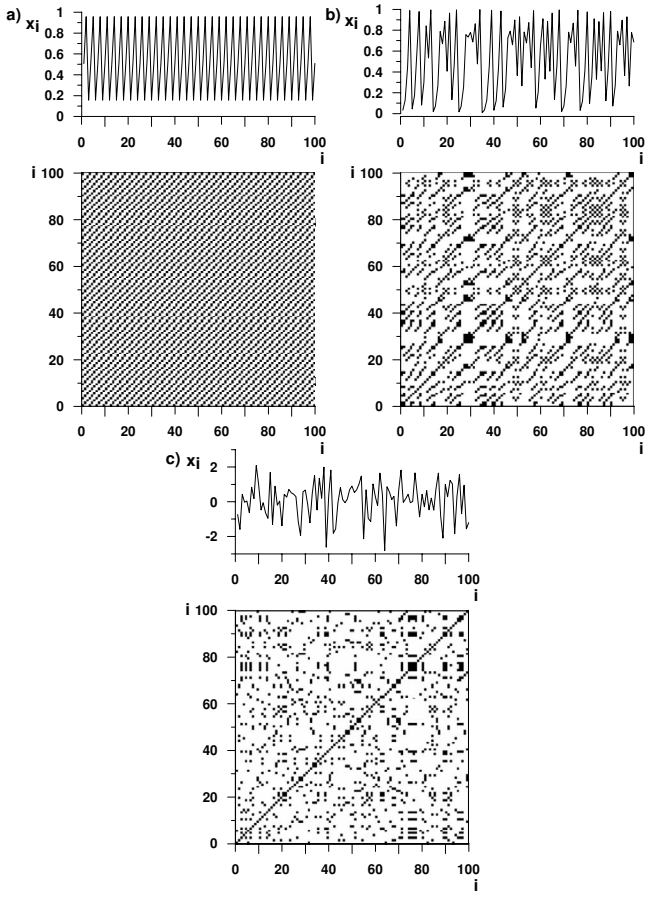

FIG. 1. Examples of the recurrence plots (lower panels) for different signals together with the raw data (upper panels): (a) a periodic signal obtained from the logistic equation for the control parameter $r=3.829$; (b) a chaotic signal obtained from the logistic equation for $r=3.9999$; (c) white noise. Note that, in the RP for the deterministic chaotic signal, short lines parallel to the main diagonal are present. Such lines do not occur in the RP of the white noise.

B. Extension of the recurrence plot quantitative analysis

As will be shown below, laminar phases of different types of intermittencies are represented by regions of the RP which have different shapes. Each of these shapes may be written into a rectangle. With the delay and embedding dimension chosen in the standard way, the shapes corresponding to the different kinds of laminar phases depend on the parameter ϵ. We found empirically that ϵ equal to 10% of the span of the reconstructed attractor allowed us to distinguish between the different types of intermittency best.

The parameter F_a is defined as the surface (measured as the number of dark points) of the area of a region corresponding to a laminar phase while F_b is the ratio of F_a to the surface of the encircling rectangle: in the case of a laminar phase in the form of a regular square, the encircling rectangle is just the border of that square. If the laminar phase is represented by a rectangle with elongated upper right corner, the encircling rectangle is the smallest rectangle into which fits the square together with the elongation. Note that—to avoid the effect of possible nonstationarity in a signal [1,13]—we take into account only these regions of the RP corresponding

to laminar phases which touch the diagonal. In a single time series, both parameters vary from laminar phase to laminar phase. To distinguish between different types of intermittency distributions of these parameters will be used below.

In certain types of intermittency (e.g., in crisis-induced chaos-chaos intermittency or when noise is present—see below) the regions representing the laminar phases are not uniform and white points appear inside them. Below we assumed that the given part of the RP is considered black if on its edge not more than single white points appear.

III. RESULTS AND DISCUSSION

A. Generic models of the laminar phases of the Pomeau-Manneville intermittencies

To obtain a recurrence plot image of the laminar phase of each type of intermittency, the generic models for Pomeau-Manneville intermittencies were analyzed. These models describe only the laminar phase so that chaotic bursts need to be simulated by a random number generator.

For type I intermittency, the laminar phase is described by the equation ([3])

$$x_{n+1} = x_n + x_n^2 + a, \tag{5}$$

where a is the distance from the critical point and here equal to 0.000 01. The value of laminar signal for this type of intermittency increases monotonically. On the recurrence plot, this signal is visible as a black square located by the main diagonal (Fig. 2). This shape reflects the dynamics of the trajectory within the laminar phase. Deep inside the laminar phase the change in trajectory position is very small so that the adjacent points are recurrent. The laminar phase in type I intermittency ends abruptly (in Fig. 2 for i about 400) in a chaotic burst. This results in a uniformly black square for a wide range of the cutoff parameter—ϵ.

The laminar phase of type III intermittency may be modeled by ([3])

$$x_{n+1} = -(1+a)x_n + ux_n^3, \tag{6}$$

where the parameters $a=0.000\,01$ and $u=0.001$. The value of the laminar signal for this case also increases but it alternates. On the recurrence plot, the laminar phase is visible as a square with an elongated upper right corner (kitelike shape—Fig. 3). In the bottom left corner of the kite there is a uniformly black incomplete rectangle with a rounded upper right corner. The upper right corner of the kitelike shape outside the rectangle is not uniformly black. It consists of parallel lines each a distance of 1 from each other (see magnification in Fig. 3). The shape and the shading are a result of the dynamics within the laminar phase. At the beginning of it, every point is close to the previous one. However, each two successive points are on the opposite sides of the ghost of the fixed point, so at the end of the laminar phase only points distanced in the time by 1 are recurrent (for the given cutoff parameter of the RP).

Type II intermittency is a two-dimensional phenomenon. Its laminar phase in polar coordinates may be described by ([3])

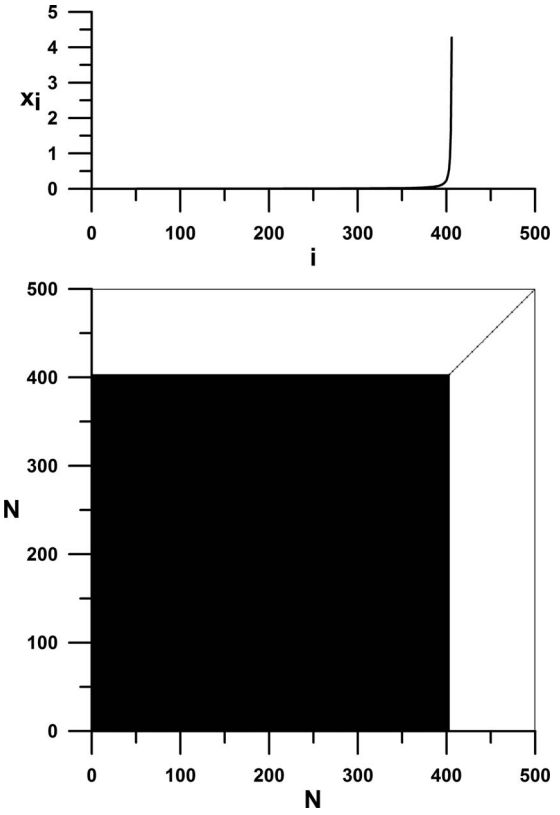

FIG. 2. The RP calculated for the time series obtained from the generic model of type I intermittency—Eq. (5). This model describes only the laminar phase of type I intermittency. For this type of intermittency, the image of the laminar phase is a black square adjacent to the main diagonal of the RP. The laminar phase ends abruptly—here at about $i=400$ (chaotic burst—not shown here).

$$r_{n+1} = (1+a)r_n + ur_n^3,$$

$$\Theta_{n+1} = \Theta_n + \Omega, \tag{7}$$

where $a=0.005$, $u=0.000\,01$, and $\Omega=0.05$. During the laminar phase the trajectory moves on a spiral. In the recurrence plot calculated for the variable $x_n=r_n\cos\Theta_n$ (or for $y_n=r_n\sin\Theta_n$) also a kitelike shape is obtained but this time its structure is different from that obtained for type III intermittency—Fig. 4. A square black shape is again visible. However, instead of a clear cut rounded upper right corner, oval white areas are embedded within the pattern. The elongated kitelike shape this time has a structure characteristic for the recurrence plot for the sinus function because, during the laminar phase, the trajectory moves on a spiral—an almost periodic behavior. Equation (7) describes only the dynamics within a laminar phase of type II intermittency. Thus, on the RP a black and white structure in the kitelike elongation of the square is visible. Changing the threshold parameter ϵ, it is possible to obtain only a fully black RP—all points in the time series are then recurrent—all belong to the same laminar phase. For models describing the complete intermittent behavior—both the laminar phases and the chaotic bursts between them—it is possible to obtain a black kitelike shape representing the laminar phases on the RP. To obtain

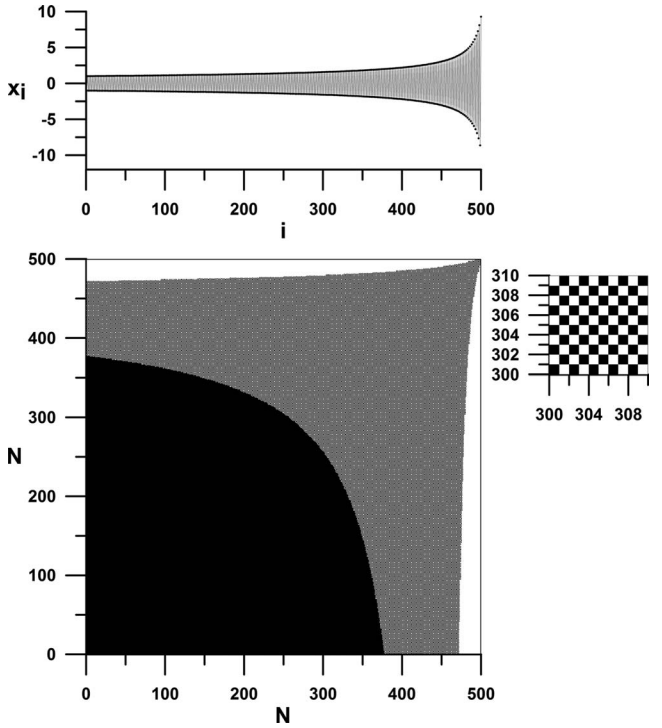

FIG. 3. RP calculated for a time series obtained from the generic model of type III intermittency—Eq. (6) (lower graph) shown with the original data (upper graph). A black square with rounded upper right corner is characteristic for the laminar phase of this type of intermittency. The elongated of the upper right corner of the pattern consists of lines parallel to the main diagonal. The distance between these lines is equal to 1—see the magnification inset.

this effect, we need to adjust the threshold parameter ϵ properly: during the chaotic bursts, the trajectory leaves the laminar region and the data points lying outside the laminar phase are not recurrent to the points within it—see Sec. III C below for further discussion.

The generic models [Eqs. (5)–(7)] are good models of the laminar phases of the Pomeau-Manneville intermittency but to study these phenomena one should take into account the dynamics during chaotic bursts. Below we present results of our analysis of different models exhibiting Pomeau-Manneville intermittencies.

B. Type I intermittency

Type I intermittency was analyzed using the logistic equation,

$$x_{i+1} = rx_i(1 - x_i), \tag{8}$$

where r is the control parameter, as a model. The analysis was performed for the values of the control parameter r slightly smaller than $r_c = 1 + \sqrt{8}$, where r_c is the critical value of the control parameter at which the period-3 window appears. The average length of the laminar phases increases as the control parameter approaches the critical value. Time series for the control parameter values 3.828 39 and 3.828 425 were generated for the first iterate (series length 15 000) and third iterate (length 5000) of the logistic map. Recurrence plots for those time series were generated. The cutoff parameter was set to 10% of the diameter of the phase space [10]. For better legibility, in the figures below, only the first 3000 (or 1000 for the third iterate) points from time series generated are shown.

In Fig. 5 it can be seen that, for the first iterate of the logistic equation, laminar phases manifest themselves on the recurrence plots as lines parallel to the main diagonal. These lines are arranged into squares and rectangles. The distance between them, within one of the rectangles, is equal to three points (Fig. 6)—a result of the proximity of the period-3 window. Note that, in this case, within each laminar phase the trajectory passes many times through three different intermittency channels in a sequence.

In the case of type I intermittency associated with a period-p orbit, the pth iterate of the map should be used to construct the recurrence plot. The squares are then mainly located along the main diagonal of the RP. They correspond to the laminar phases. Each square at the diagonal is a representation of a trajectory crossing a single channel. When the pth iterate is used, well defined black squares are obtained. Figure 7 depicts the pattern obtained for the third iterate of the logistic map for two values of the control parameter.

Additional squares appear at a distance from the main diagonal when two squares situated at the main diagonal have the same length (8 and 9 in Fig. 8). These squares are the representation of different trajectories traversing the same intermittency channel which makes them pass close to each other in phase space. Rectangles are situated at a distance from the main diagonal (Fig. 8). They appear at the crossing of the extensions of the edges of the squares. However, not every pair of the edges of squares leads to the creation of a rectangle. For a rectangle to appear, both squares must correspond to the same intermittency channel. When two squares correspond to different intermittency channels, the trajectory corresponding to one of the squares is close to the one of the fixed points, and in the case of the second square, it is close to another fixed point. However, these fixed points are not close to each other in phase space so the points of the trajectory within different intermittency channels are not recurrent to each other.

The distribution of the area of the black squares for the recurrence plots of the time series obtained from the third iterate of the logistic equation is presented in Fig. 9. As can be seen, the distribution of the area is similar to the distribution of the laminar phases of type I intermittency. The maximum length of the laminar phase is $l_{max} = (r_c - r)^{-1/2}$. If the black squares and rectangles correspond to laminar phases, the maximum value of square root of the area of squares lying at the main diagonal ($\sqrt{F_{a_{max}}}$) should be equal to the l_{max}. One can see in Fig. 9 that $3\sqrt{F_{a_{max}}}$ has a similar value to that of l_{max}. For example, in Fig. 9(a) [for the approximate analytic model of Eq. (3.15) from Ref. [21]], we obtain from Eq. (3.15) of Ref. [21] $l_{max} = 165$ while for the data obtained from the logistic map using our method l_{max} equals 180 and in part (b) of this figure 686 vs 750, respectively.

To verify the assumption that the distribution of $\sqrt{F_a}$ is similar to the distribution of the laminar phase length $P(l)$, a

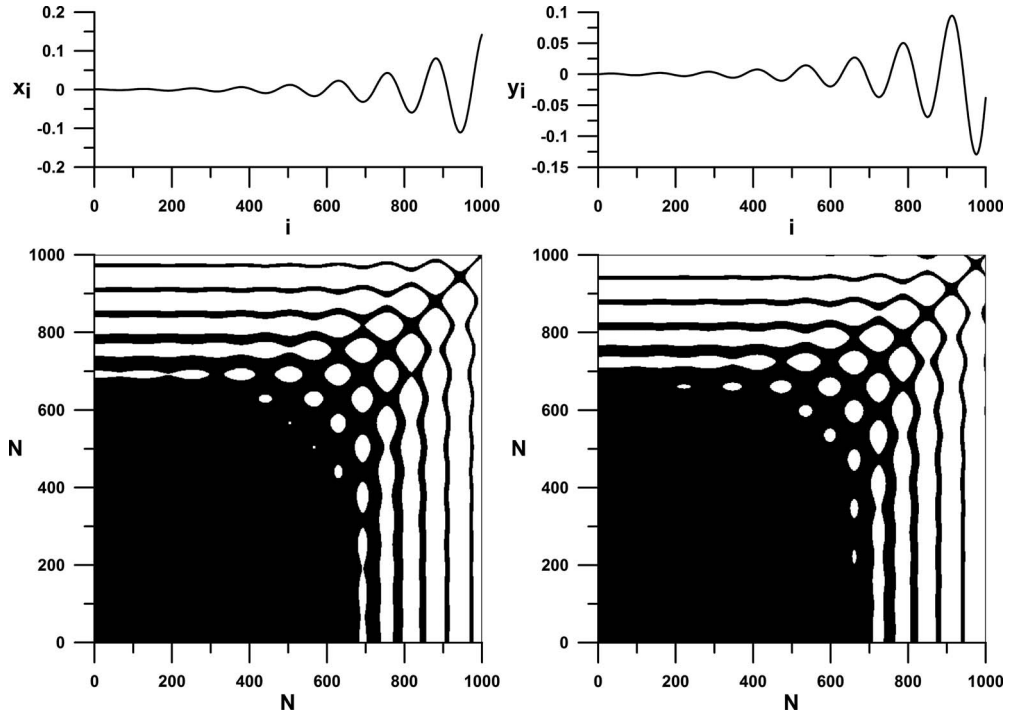

FIG. 4. RP calculated for a time series obtained from the generic model of type II intermittency—Eq. (7) (lower graphs) shown with the original data (upper graphs). The left column depicts results for the x variable while the right—for the y variable of the model. For the generic model, a black square with perforated upper and right edges is the characteristic shape for the laminar phase of this type of intermittency. The perforation structure is due to the periodic behavior at the end of the laminar phase and is similar to the pattern obtained for harmonic functions.

time series from the original model used by Hirsh [21],

$$x_{i+1} = x_i + x_i^2 + a, \tag{9}$$

was calculated. This equation may be treated as a simplified model for type I intermittency [3,21]. From this equation only laminar phases can be generated and the reinjection process has to be simulated. Following [21], we assumed that this equation is valid only for $x_i \in (-x_0, x_0)$. Outside this range the dynamics was modeled by the logistic equation with the control parameter $r=3.999$ (a chaotic state). We choose $x_0=0.07$ and $a=0.001$. A time series of 40 000 points was generated with 1246 laminar phases. For this time series, the RP was calculated and the distribution of $\sqrt{F_a}$ was obtained. One can see in Fig. 10 that the shape of the distribution of $\sqrt{F_a}$ is consistent with the theoretical curve given by Eq. (3.15) in Ref. [21]. Note that the discrepancy between the analytically obtained laminar phase distribution and the one found by our method is due to the difference in the models used (the simplified model of Ref. [19] and the lo-

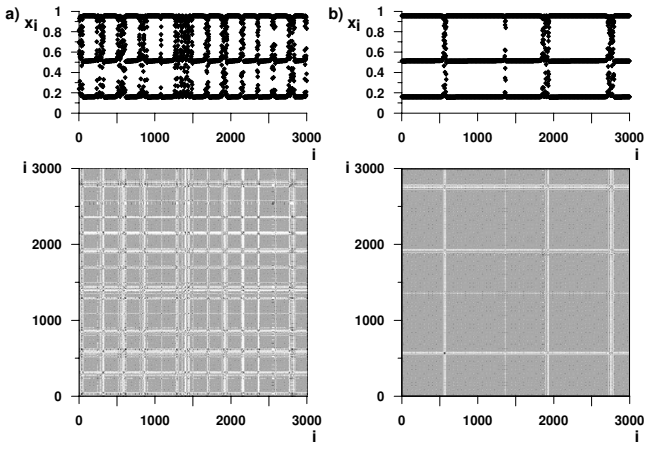

FIG. 5. Recurrence plots and the time series calculated using the logistic equation for the control parameter r smaller than r_c. (a) $r=3.828\,39$; (b) $r=3.828\,425$.

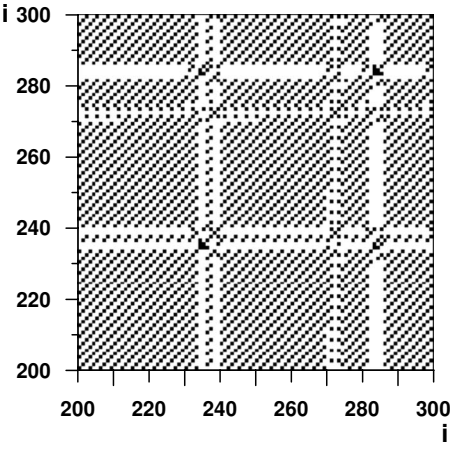

FIG. 6. Enlargement of the RP shown in Fig. 5(a). When a laminar phase occurs, lines parallel to the main diagonal, forming squares and rectangles, are present in the RP.

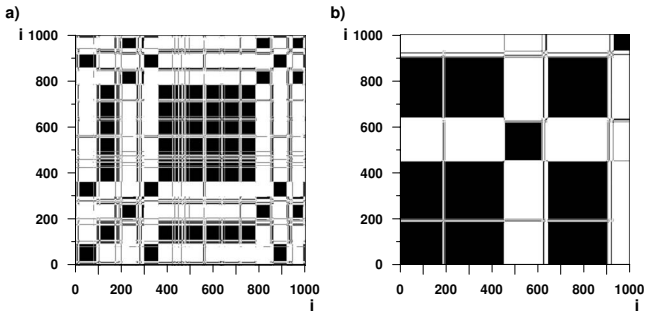

FIG. 7. Recurrence plots of the signals obtained from the third iterate of the logistic equation for the same control parameter values as in Fig. 5: (a) $r=3.828\,39$; (b) $r=3.828\,425$.

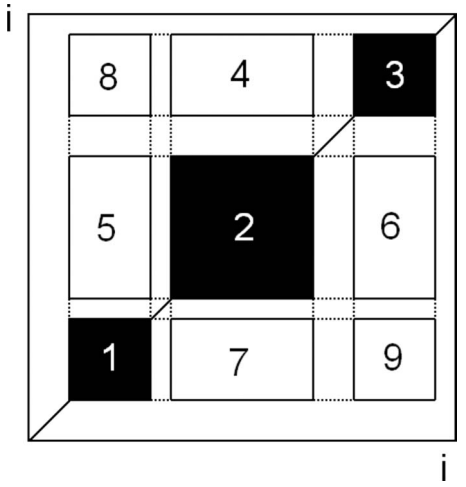

FIG. 8. Schematic illustrating the origin of the recurrence squares and rectangles for type I intermittency. Appearance of squares 8 and 9 is a consequence of the occurrence of the squares 1 and 3—images of the laminar phases of the same length. The rectangles 4 and 6 are a result of the occurrence of the squares 2 and 3 each with a different length of the side, similarly, rectangles 5 and 7.

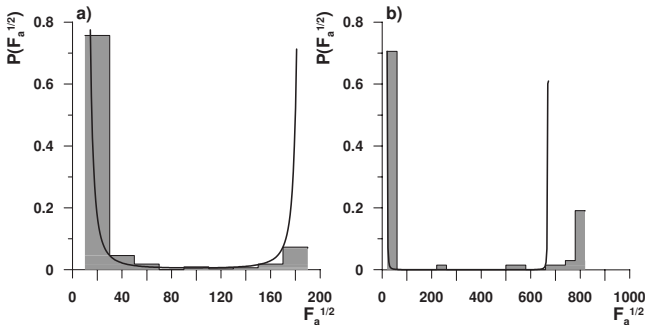

FIG. 9. The histograms of $\sqrt{F_a}$ for the time series with type I intermittency: part (a) $r=3.828\,39$, the number of laminar phases was 329; part (b) $r=3.828\,425$, the number of laminar phases—68. The maximum lengths of the laminar phases obtained analytically (solid curve) using Eq. (3.15) in Hirsch *et al.* [21] were equal to 165 and 686, respectively.

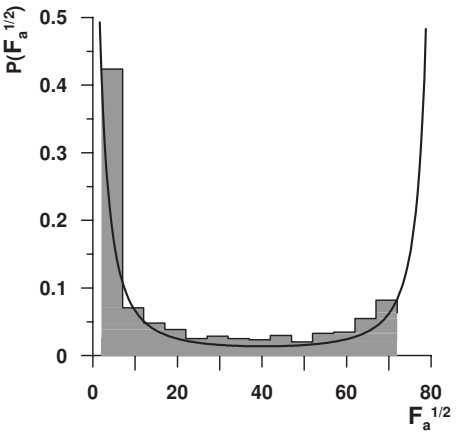

FIG. 10. The distribution of $\sqrt{F_a}$ obtained from the RP for the simple model of the type I intermittency for $x_0=0.07$ and $a=0.001$. Black line: analytical result—according to Eq. (3.15) in Hirsch *et al.* [21].

gistic map used here). Also, there is a difference in the limits of the laminar phase assumed in the two methods. These limits define the length of the laminar phase. In the case of the recurrence diagram, the limits of the intermittency channel are a complex and unknown function of the cutoff parameter ϵ. The same explains the discrepancies found in the preceding paragraph.

The distribution of the parameter F_b was calculated (Fig. 11). It can be seen that for this type of intermittency F_b is equal to 1 for all laminar phases. For $F_b=1$, all squares touching the main diagonal of the RP are uniformly black.

C. Type II intermittency

Type II intermittency is due to the subcritical Hopf bifurcation. In this bifurcation, a stable fixed point and an unstable limit cycle corrupt into a single unstable fixed point. The laminar phase occurs when the trajectory of the system is injected close to that unstable fixed point. The trajectory then forms a spiral outward from the fixed point. When the trajectory leaves this region the chaotic phase occurs ending with a reinjection into the part of the phase space between the fixed point and an unstable limit cycle. In contrast to the generic model of type II intermittency (Sec. III A), which

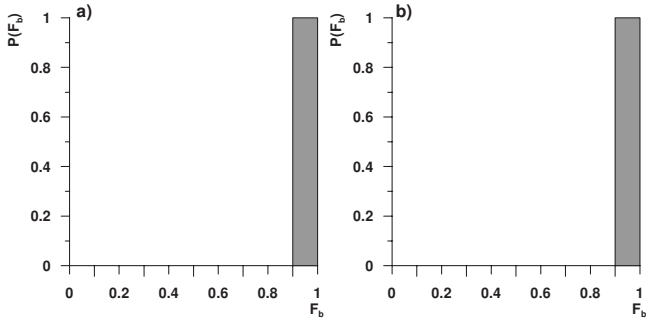

FIG. 11. The distribution of the parameter F_b for type I intermittency: (a) $r=3.828\,39$, the number of laminar phases in the time series is 329; (b) $r=3.828\,425$, the number of laminar phases—68.

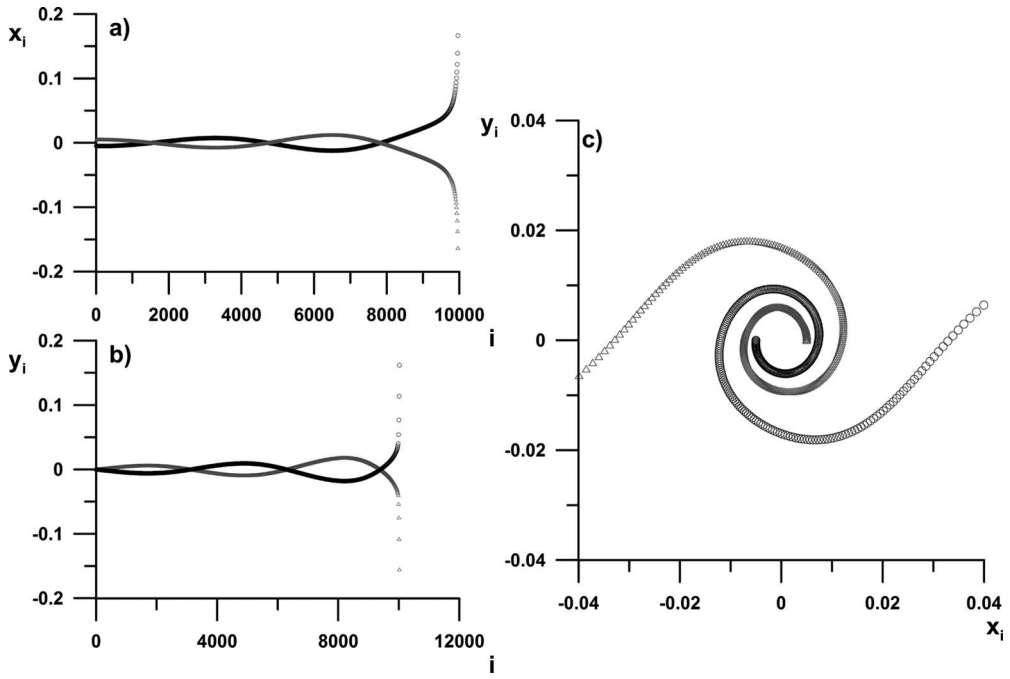

FIG. 12. Trajectory during laminar phase of type II intermittency obtained from Eq. (10) with the following parameters: $b=0.14$, $\gamma=0.02$, $\epsilon=0.001$, and $\mu=0.0001$. The data for the x and y variables are shown in the left panels. Each thin line and thick line, respectively, depict the data for separate laminar phases which are interleaved. The right panel depicts the shape of the trajectories with the arrows marking the direction of motion.

describes the dynamics within a single laminar phase, in systems exhibiting the complete intermittency laminar phases may be intertwined: adjacent data points in the time series belong to different spiral trajectories [22].

A time series characteristic for type II intermittency was obtained from the equations presented in Ref. [22]:

$$x_{i+1} = -[(1+\mu+\gamma)x_i + x_i^3]\exp(-bx_i^2) + \gamma x_i + \epsilon y_i,$$

$$y_{i+1} = -[(1+\mu+\gamma)y_i + y_i^3]\exp(-by_i^2) + \gamma y_i - \epsilon x_i. \quad (10)$$

For $b < 1/1-(1/2)\epsilon^2+\gamma$ [22] a subcritical Hopf bifurcation occurs allowing type II intermittency to occur. Here, the parameters b, γ, and ϵ were set equal to $b=0.14$, $\gamma=0.02$, $\epsilon=0.001$, and $\mu=0.0001$ [22].

The peculiar property of the model given by Eq. (10) is that, during intermittency, two laminar phases are intertwined—every other point of the trajectory is associated with the same spiral. Figure 12(c) depicts two successive laminar phases with the data shown for the x variable in Fig. 12(a) and for the y variable in Fig. 12(b). Consequently, in the RP analysis only every other point from the time series was used. The RP of the single laminar phase is presented in Fig. 13. As described in Sec. III A, for type II intermittency, using an appropriate value of the threshold parameter ϵ one obtains a uniformly black kitelike shape for the laminar phase—Fig. 13(a). This typically occurs for ϵ of the order of 10% of the attractor diameter. When ϵ is decreased from this value, the structure characteristic for the harmonic motion occurring during the type II intermittency laminar phase will appear [the kitelike elongation of the square—Fig. 13(b)] and allows to recognize the type of intermittency unambiguously.

The RP ($m=2$, $\tau=1$, $\epsilon=0.1$) for the first 1000 points of the time series calculated as every other point from x series obtained from Eq. (10) is presented in Fig. 14(a). The squares and rectangles with an elongated upper right corner (a uniformly black kitelike shape) characteristic for the laminar phases are present. The choice of values of the ϵ parameter assures that they are uniformly black. For the RP of the complete series, the length of which was 10 000 points, a histogram of $\sqrt{F_a}$—a measure of the laminar phase length—was created for the black fields [Fig. 14(b)]. For type II intermittency, the probability distribution of the length of the laminar phases is [3]

$$P(l) \propto \frac{\epsilon^2 \exp(4\epsilon l)}{[\exp(4\epsilon l)-1]^2}. \quad (11)$$

This analytical function was fitted to the histogram of the $\sqrt{F_a}$. In Fig. 14(b) it can be seen that this histogram has a shape characteristic for the histogram of the laminar phases of type II intermittency. The correlation coefficient of the fit is equal to $R^2=0.99$. Also the distribution of F_b [Fig. 14(c)] has a shape that is significantly different from that obtained for type I intermittency (Fig. 11).

D. Type III intermittency

Type III intermittency occurs simultaneously with the reverse period doubling bifurcation [3]. In this bifurcation, an unstable periodic orbit collides with a stable periodic orbit

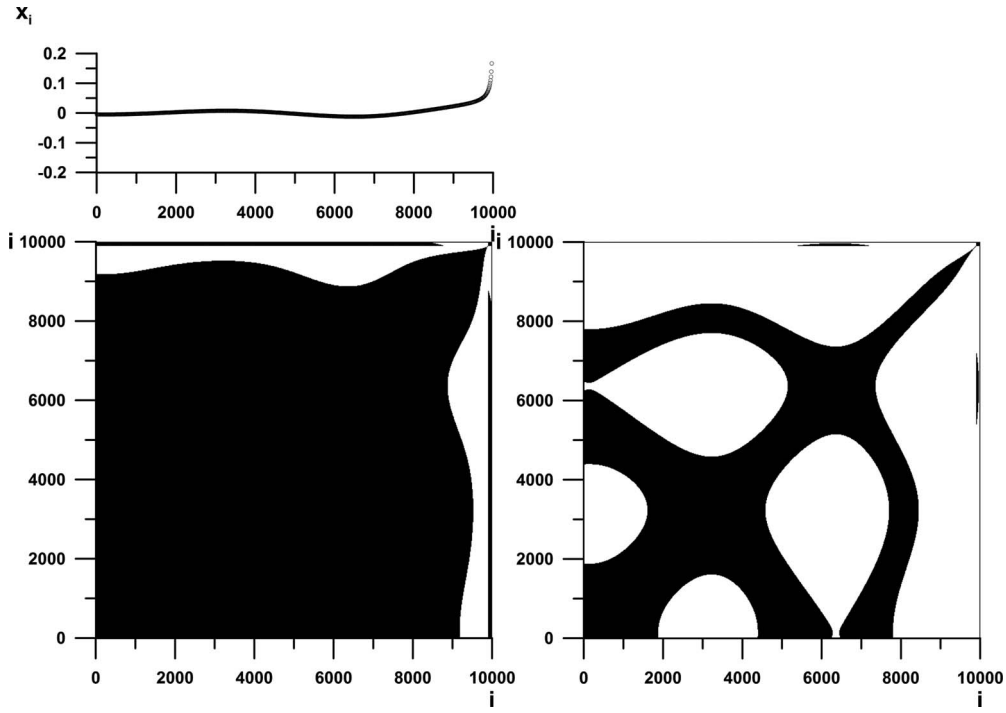

FIG. 13. The RPs of a single laminar phase of type II intermittency obtained from Eq. (10). The parameters of the RP were set to $m=2$, $\tau=1$, and $\epsilon=0.1$ in the left RP and $\epsilon=0.01$ in the right RP. In the right RP, the white regions in the kitelike elongation of the upper right corner of the square—characteristic for type II intermittency is visible—for comparison see Fig. 4 and discussion in the text.

which has a period one half of that of the unstable orbit. As a result of the bifurcation, both orbits are superseded by an unstable periodic orbit with the smaller period.

Type III intermittency was obtained using one of the pair of equations used for the generation of type II intermittency but with the coupling omitted:

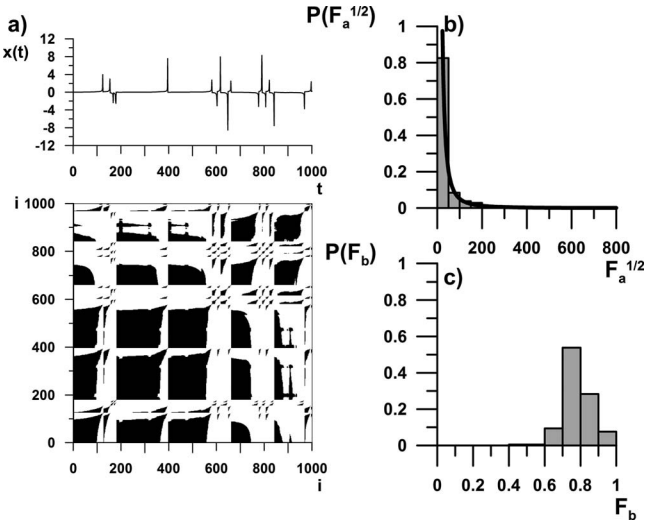

FIG. 14. (a) RP ($m=2$, $\tau=1$, $\epsilon=0.1$) and the time series for type II intermittency obtained from Eq. (10) (parameters: $b=0.14$, $\gamma=0.02$, $\epsilon=0.001$, and $\mu=0.0001$). (b) Histogram of $\sqrt{F_a}$, the number of laminar phases—213 [black line—the analytical distribution of the laminar phases for the type II intermittency—Eq. (11)]; (c) the probability distribution of F_b.

$$x_{i+1} = -[(1+\mu+\gamma)x_i + x_i^3]\exp(-bx_i^2) + \gamma x_i. \quad (12)$$

For $b=0.14$, $\gamma=0.02$, and $\mu=0.005$ type III intermittency occurs in this system [22]. A time series of 10 000 points was generated and the RP for this data was calculated. Figure 15(a) depicts the RP for the first 1000 points from that series. The same parameters of the RP as those used for the analysis of intermittency type I were set.

Laminar phases of type III intermittency are represented in the recurrence plots as squares and rectangles with a rounded upper right corner [Fig. 15(a)]. The genesis of these squares and rectangles is the same as for type I intermittency. The distribution of the areas of the black fields of the recurrence plot for type III intermittency is presented in Fig. 15(b). To this distribution the analytical function given by the equation [3]

$$P(l) \propto \frac{\epsilon^{3/2}\exp(4\epsilon l)}{[\exp(4\epsilon l)-1]^{3/2}} \quad (13)$$

was fitted. As can be seen, the histogram of the $\sqrt{F_a}$ for type III intermittency is similar to the theoretical distribution of the laminar phases for that intermittency. The correlation coefficient of the fit is equal to $R^2=0.93$. The distribution of the F_b parameter is different than that for the intermittencies discussed above [Fig. 15(c)].

E. Chaos-chaos intermittency

One of many different types of chaos-chaos intermittency is caused by an interior crisis. In deterministic dynamical systems, such a crisis is a collision between a chaotic attrac-

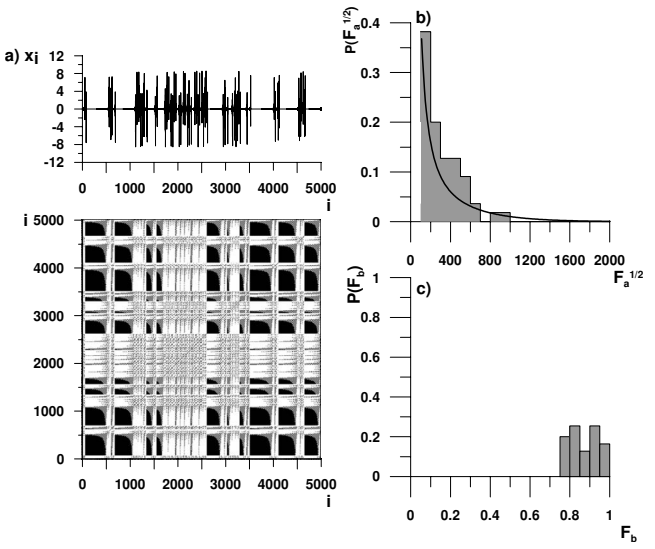

FIG. 15. (a) RP and data for type III intermittency (parameters: $b=0.14$, $\gamma=0.02$, and $\mu=0.005$); RP parameters: $m=2$, $\tau=1$, and $\epsilon=0.1$. (b) Histogram of the $\sqrt{F_a}$; the number of laminar phases—55 [black line—the analytical distribution of the laminar phases for the type III intermittency—Eq. (13)]; (c) the probability distribution of F_b.

tor and a coexisting unstable fixed point or an unstable periodic orbit [1]. The interior crisis in the logistic map occurs when the chaotic attractor, resulting from period doubling of a periodic window, collides with an unstable orbit which coexists with it and lies inside the attraction basin but does not belong to the attractor. This kind of crisis occurs for the logistic equation at the large control parameter end of every periodic window.

In the case of the periodic-3 window of the logistic map, the three parts of the chaotic attractor appear due to a period doubling bifurcation. When the critical value of the control parameter corresponding to the internal crisis is attained, the trajectory occasionally slips out of the period doubled period-3 orbit (chaotic orbit). This occurs as an effect of the collision between the chaotic attractor and the unstable periodic orbit, which was created by a saddle-node bifurcation when the period-3 window was created. In the chaos-chaos intermittency a regular laminar phase does not occur. Intermittency in this case means that the trajectory repeatedly resides within the precrisis attractor (laminar phase) and repeatedly visits the part which was formed during the crisis (chaotic phase) [1].

Chaos-chaos intermittency induced by an interior crisis was obtained from the logistic map for the control parameter $r=3.857$. In Fig. 16, the RP of that signal is presented for the third iterate of the logistic equation (only the first 1000 iterates are depicted). In this case, the RP for this type of intermittency is similar to that obtained for type I intermittency. However, when a magnification of the RP is examined (Fig. 17), the lines forming a black field of the RP calculated for the first iterate of the map are found to be not continuous—in contrast to such lines for the case of type I intermittency. Also, for the third iterate in the case of chaos-chaos intermittency, the black fields characteristic for the laminar phases are not uniformly black.

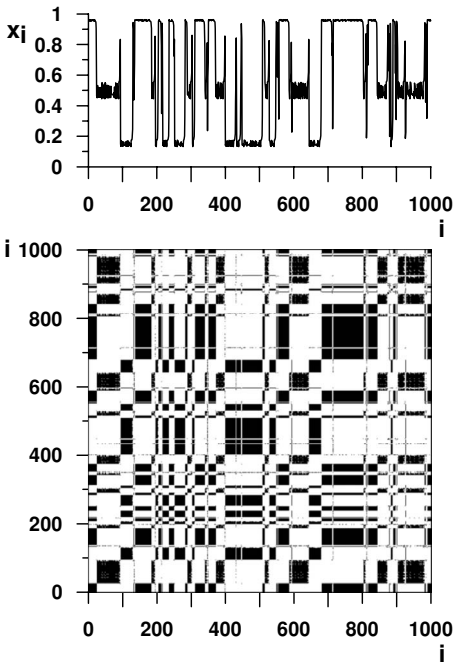

FIG. 16. The RP for chaos-chaos intermittency induced by an interior crisis. The time series was obtained from the third iterate of the logistic equation for control parameter $r=3.857$.

The distribution of the parameter F_a was calculated for chaos-chaos intermittency. In Fig. 18 it can be seen that, although the RP of this type of intermittency has many similarities to that obtained for type I intermittency, the distributions of $\sqrt{F_a}$ and F_b have now distinctly different shapes (compare Figs. 9 and 11). Note that the distribution of F_b for chaos-chaos intermittency may be mistaken for that of type II. However, these two types of intermittency may still be distinguished by the different shapes of the black fields in the RPs.

F. Intermittency in systems with continuous time

Systems with the continuous time exhibiting intermittencies type II and type III were examined. The time series with

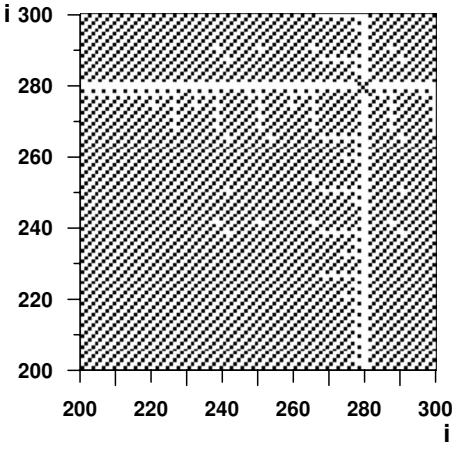

FIG. 17. Magnification of the RP obtained from the first iterate of the logistic equation for control parameter $r=3.857$—an example of a laminar phase.

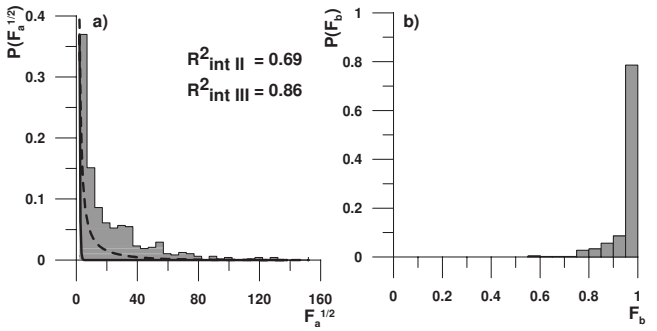

FIG. 18. (a) The distribution of $\sqrt{F_a}$ obtained from chaos-chaos intermittency (logistic equation; $r=3.857$). Solid line—distribution of the laminar phases for type II intermittency; dashed line—distribution of the laminar phases for type III intermittency. (b) The probability distribution of F_b.

type II intermittency was obtained from the system

$$\frac{d^3X}{dt^3} + \eta\frac{d^2X}{dt^2} + \nu\frac{dX}{dt} + \mu X + k_1X^2 + k_2\left(\frac{dX}{dt}\right)^2 + k_3X\frac{dX}{dt} + k_4X\frac{d^2X}{dt^2} + k_5X^2\frac{d^2X}{dt^2} = F\cos(\omega t). \quad (14)$$

For that system Richetti *et al.* [23] found that for the parameters $F=0.5$, $\omega=15$, $\eta=1$, $\nu=1.2$, $k_1=-100$, $k_2=120$, $k_3=0$, $k_4=-20$, $k_5=100$, and $\mu=1.25$ type II intermittency occurs. The characteristic shape of the trajectory for this type of intermittency is visible only in the stroboscopic section [Fig. 19(b)] of the raw data [Fig. 19(a)] (see [23] for details). To examine the image of the laminar phases on the RP, only

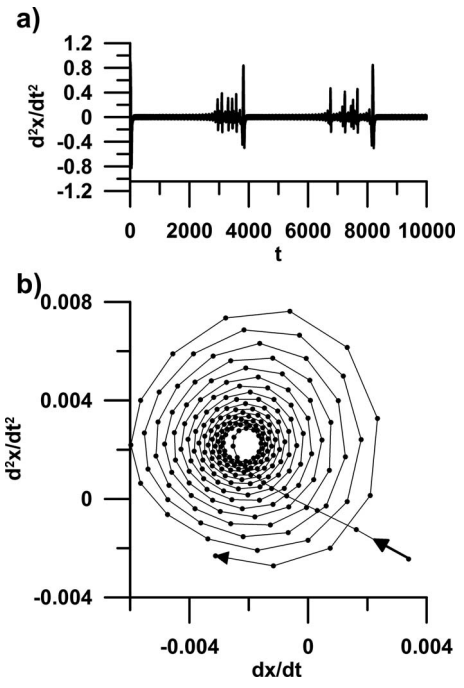

FIG. 19. The characteristic shape of the trajectory for type II intermittency is visible only in the stroboscopic section—(b) of the raw data obtained from Eq. (14)—(a) (see [23] for details).

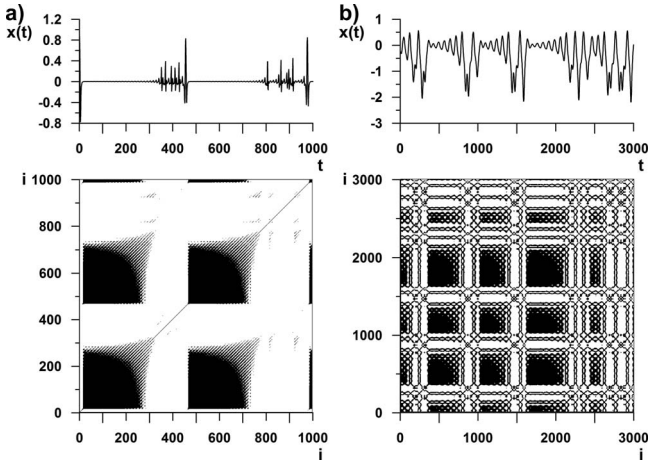

FIG. 20. RP of systems with continuous time: part (a)—type II intermittency [Eq. (14)] and part (b)—type III intermittency [Eq. (15)]. For type II intermittency, the characteristic kitelike shape is visible. The distances between the lines forming the elongated upper right corner of the pattern are due to the sampling rate (integration time step). For type III intermittency, the shape characteristic for it is also visible—a square with a rounded upper right corner and perforated outer edges.

points from the stroboscopic section were used. The time delay $\tau=3$ was selected using the MIF, and the embedding dimension $m=4$—using the false nearest neighbors method.

The time series with type III intermittency was obtained from the system

$$\frac{d^2X}{dt^2} + 0.2\frac{dX}{dt} + X + 1.5X^2 + 0.5X^3 = FX\cos(\omega t). \quad (15)$$

Type III intermittency in this system occurs for $F=0.85$ and $\omega=1.6852$ [24]. For this system the appropriate embedding and delay are $\tau=10$ and $m=3$.

In Fig. 20 the recurrence plots obtained for the time series from both systems can be seen. For the type II intermittency the characteristic kitelike shape of the laminar phase is visible [Fig. 20(a)], however, the elongated upper right corner is not solid black as it was for the type II intermittency obtained from the discrete-time system. Also for the type III intermittency obtained from the system with the continuous time the shape of the laminar phase is slightly different than obtained for a system with discrete time. In the present case, the rounded upper right corner characteristic for the type III intermittency is visible. Also the kitelike elongation of the square consisting of lines parallel to the main diagonal is present. However, now the space between lines is greater than 1. This makes the image of this intermittency similar to that for type II intermittency. However, while the larger distance between these lines in the case of type II intermittency is due to the spiraling motion of the state point while for type III intermittency the distance between the lines is due to the sampling rate. Changing the sampling rate during data collection for type II intermittency has no effect on the distance between the lines parallel to the main diagonal. For type III intermittency, to obtain the distance between the parallel lines of 1 one needs to choose the proper sampling rate.

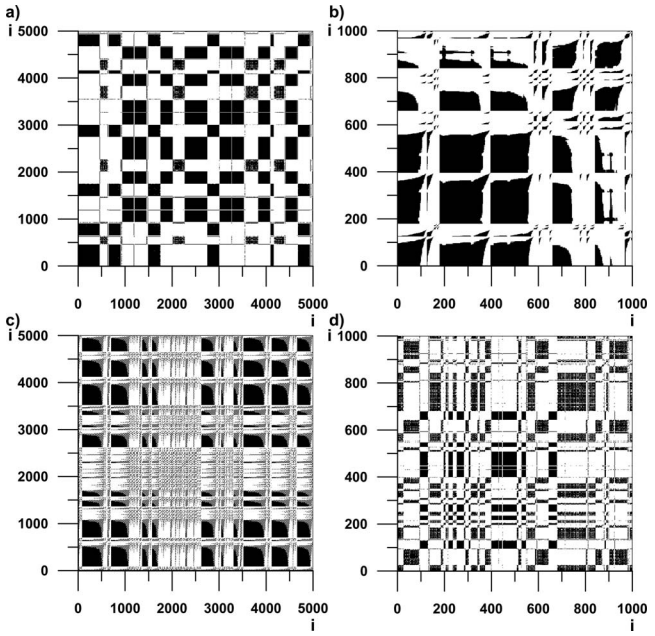

FIG. 21. The recurrence plots of four different types of intermittencies with measurement noise added to the time series. The noise level was 10%. (a) Type I intermittency $r=3.828\,425$; (b) type II intermittency; (c) type III intermittency; (d) chaos-chaos intermittency $r=3.857$.

Thus, in spite of the seemingly ambiguous shape of the RP patterns, it is possible to distinguish between type II and type III intermittency for systems with continuous time.

G. Effect of measurement noise

The effect of measurement noise on the performance of our method presented above was analyzed. To all time series used for the previous calculations, measurement noise in the following form was added:

$$x_{i,\xi} = x_i(1 + \xi p), \tag{16}$$

where ξ is a random number uniformly distributed in the range [0,1], and p the level of noise (in percent). We applied noise of up to $p=30\%$. Figures 21–23 demonstrate the effect of 10% measurement noise on the different types of the intermittencies studied here. It can be seen that noise of that level causes the squares and rectangles characteristic for the laminar phases to be no longer uniformly black but that white points occur inside them. However, the patterns characteristic for each type of intermittency remain recognizable. Also, in spite of the noise, the shapes of the histograms of $\sqrt{F_a}$ were also preserved for the types of intermittency examined here.

Using just the images of the RP pattern obtained (Fig. 21), we can immediately distinguish type II and type III unambiguously. Type I intermittency and chaos-chaos intermittency in the presence of noise appear similar. To distinguish them, the histograms of $\sqrt{F_a}$ should be used—for the case of the period-3 window of the logistic map given here as an example—with the third iterate of the map. In Fig. 22(a) the characteristic for type I intermittency U shape is depicted,

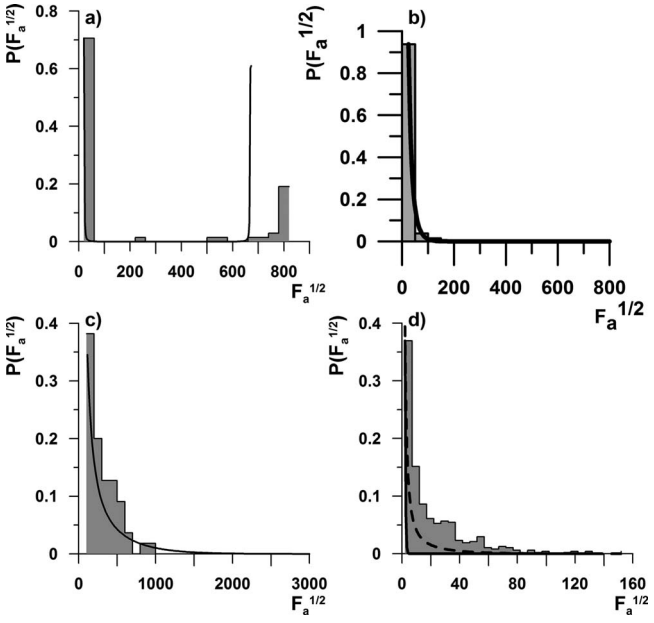

FIG. 22. The distribution of $\sqrt{F_a}$ for different types of intermittencies obtained from the RPs presented in Fig. 21. Noise level—10%. (a) Type I intermittency $r=3.828\,425$ [solid curve—the analytical distribution of the laminar phases for the simple model of type I intermittency—Eq. (9)]; (b) type II intermittency [solid curve—the analytical distribution of the laminar phases for the type II intermittency—Eq. (11)]; (c) type III intermittency [solid curve—the analytical distribution of the laminar phases for the type III intermittency—Eq. (13)]; (d) chaos-chaos intermittency $r=3.857$ (solid line—distribution of the laminar phases for type II intermittency; dashed line—distribution of the laminar phases for type III intermittency).

while in the rest of the figure for the other types of intermittencies the distributions of $\sqrt{F_a}$ have other shapes—also characteristic for each of them. On the other hand, the histograms of F_b in the presence of noise become similar to each other (Fig. 23).

If the first iterate of the logistic map needs to be examined, to distinguish between the type I or chaos-chaos intermittency, a magnification of the images of the laminar phases in the RP should be used. As can be seen in Fig. 24(a), for type I intermittency lines parallel to the main diagonal are present in the RP. In the case of measurement noise, in these lines gaps appear [Fig. 24(b)]. For the chaos-chaos intermittency the lines parallel to the main diagonal are broken even in the case without noise. But, as can be seen in Fig. 24(c), many of these lines are shifted with respect to each other. In the case of chaos-chaos intermittency with measurement noise, the gaps in the parallel lines are longer than for the case without noise and parallel displacements between neighboring parts of the lines are visible also—see the parts of Figs. 24(c) and 24(d) marked by gray rectangles. We were able to distinguish all the kinds of intermittency discussed here up to the level of 30% of measurement noise in this way.

H. Application to heart rate variability data

The method presented above was used to detect intermittency in recordings of heart rate variability (HRV). Although

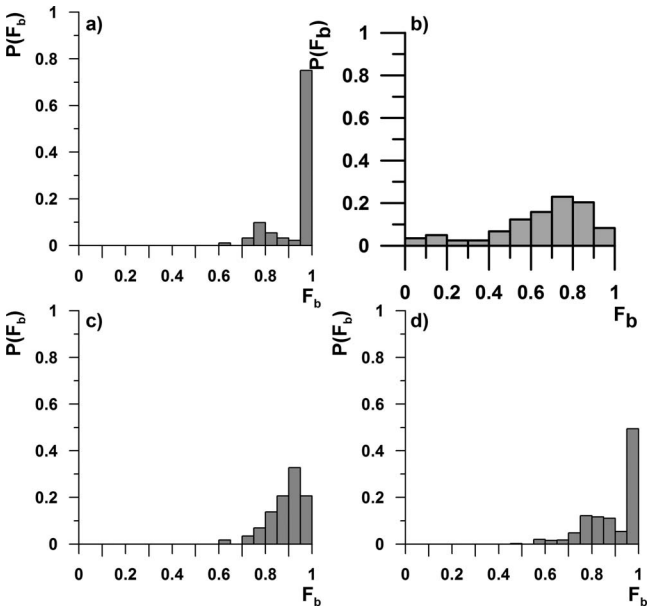

FIG. 23. The distribution of F_b for different types of intermittencies with measurement noise added to the time series. Noise level—10%. (a) Type I intermittency $r=3.828\,425$; (b) type II intermittency; (c) type III intermittency; (d) chaos-chaos intermittency $r=3.857$.

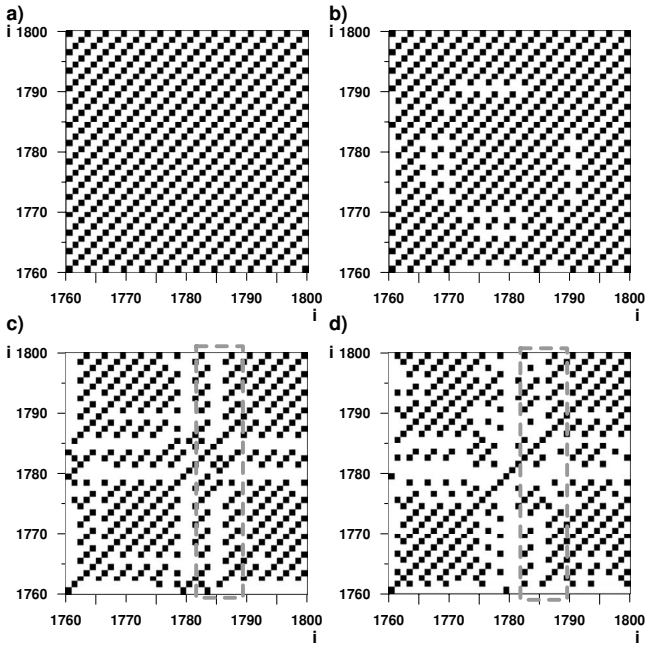

FIG. 24. The comparison between type I intermittency without (a), and with (b) measurement noise, with chaos-chaos intermittency without (c) and with (d) noise for the first iterate of the logistic equation. For type I intermittency, lines parallel to the main diagonal are visible. In case of noise these lines have gaps. For chaos-chaos intermittency the lines parallel to the main diagonal are also visible but even without noise these lines have gaps. For chaos-chaos intermittency parts of the lines are shifted with respect to each other. The gray rectangles mark corresponding patterns in the two cases.

the ECG itself is a continuous time signal, the heart rate variability is measured as a time series of the time intervals between heart beats—the RR intervals. The latter series represents a discrete time system (a point process): each element of the series is the time between specific maxima (the R peak) of the ECG trace. Recently, using a method involving the calculation of the average deviation of the data in a short sliding window, type I intermittency was found in 24 h recordings of heart rate variability of certain patients [25,26] but not in recordings of the HRV of normal subjects. Here, we demonstrate the applicability of our method to such data using a 20 000 data-point long fragment of a 24 h recording registered for a postmyocardial infarction patient. In the whole 24 h recording, there were less than 1000 premature ventricular beats so that the case may be classified as sinus rhythm. A fragment of the data is shown in the upper panel of Fig. 25(a) together with the corresponding RP just below. The parameters of the RP used in this case were $m=6$ (this value was obtained as the best embedding dimension by the false nearest neighbors method), $\tau=1$, and $\epsilon=300$. The value of the threshold parameter was chosen as 10% of the span of the reconstructed six-dimensional phase space. For this value of the embedding dimension, the span of the reconstructed phase space was slightly above 2900. Black squares and rectangles—the pattern characteristic for type I intermittency—may be seen in the RP. The distributions of the parameters $\sqrt{F_a}$ and F_b are shown in Figs. 25(b) and 25(c), respectively. The solid curve in Fig. 25(b) depicts the best fit of the analytic expression to the distribution: Eq. (3.15) in Ref. [21]. It can be seen that maximum laminar phase length of the fitting curve agrees rather well with the first right peak in the measured distribution but that the overall shape of the latter departs from the shape predicted by simple theory. The exact shape of the distribution obtained depends on several factors including the symmetry of the map close to the bifurcation point, on reinjection probability density and on the definition of the end of the intermittency channel used in the algorithm for the recognition of laminar phases. The properties of the map that is responsible for the intermittency in RR intervals are unknown so we can only surmise as to reasons for the shape of the laminar phase distribution. The long tail and additional peaks in this distribution were explained in Refs. [26,27]. On the other hand, the distribution of F_b is exactly such as one would expect for type I intermittency with noise and may be used to decide that this phenomenon indeed occurs in the data analyzed. To double check if this is the case, we used that same method of determining the distribution of laminar phases as was used in Ref. [25]. The results are shown in Fig. 26. It can be seen that the distribution measured here and the one found by the previous method coincide. Note that here we used just a 20 000 data-point fragment of the 24 h heart rate variability recording while in Ref. [25] the complete set was used.

As additional proof that the dynamics of the heart rate presented in this section corresponds to a type I intermittency, we used the RP to detect and extract two consecutive laminar phases from the time series of RR intervals. In Fig. 27(a) we show the RP formed by 100 consecutive RR intervals from the same recording as discussed above. A pattern characteristic for four laminar phases is present in the RP. We

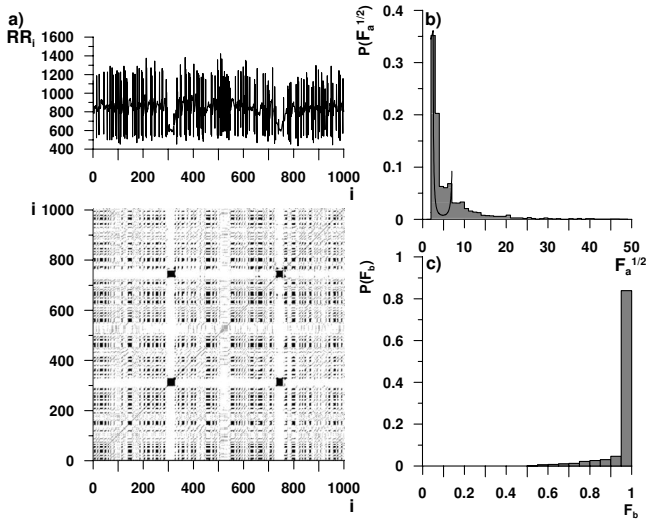

FIG. 25. Application of the method to heart rate variability data. Part (a) upper panel: the RP of a time series extracted from a 24 h recording of the heart rate (morning hours). For legibility, only a 1000 data-point long fragment of the RP is presented; the complete data set analyzed by the extended recurrence plot analysis was 20 000 data points long. Lower panel: the recurrence plot of the data in the upper panel obtained with the parameters $m=6$, $\tau=1$, and $\epsilon=300$; part (b): the distribution of the parameter $\sqrt{F_a}$ for the complete data set; part (c): the distribution of F_b for the complete data set. The total number of laminar phases was 1038.

used the limits of the squares situated at the diagonal of the pattern to identify the indices corresponding to the laminar phases. In part (b) of the same figure, the fragment of the time series corresponding to the RP is presented with the laminar phases marked by vertical dashed lines, and in part (c)—the first return map formed from these laminar phases; the arrows depict the direction of motion. In the latter figure, two passages through the intermittency channel are seen as expected in type I intermittency—an indication of the proximity to the saddle-node bifurcation. The small wiggles in the trajectory seen during the traversing of the channel are due to noise. Note that—just as in the data of Ref. [25]—the laminar phases are short: their length does not exceed ten RR intervals. This is also seen in Fig. 26.

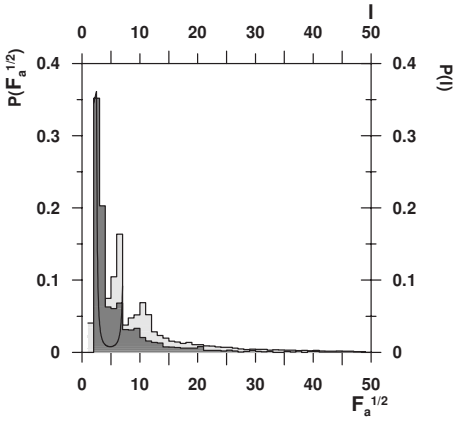

FIG. 26. A comparison of the results presented in Fig. 25(b) with results presented in Żebrowski [25]. Light gray—results from Żebrowski [25] (for this part of the figure the y axis is on the right side of the plot and the x axis—at the top); dark gray—results presented in Fig. 25(b); black line—distribution of the laminar phases for the simple model of type I intermittency [Eq. (3.15) in Hirsch *et al.* [21]].

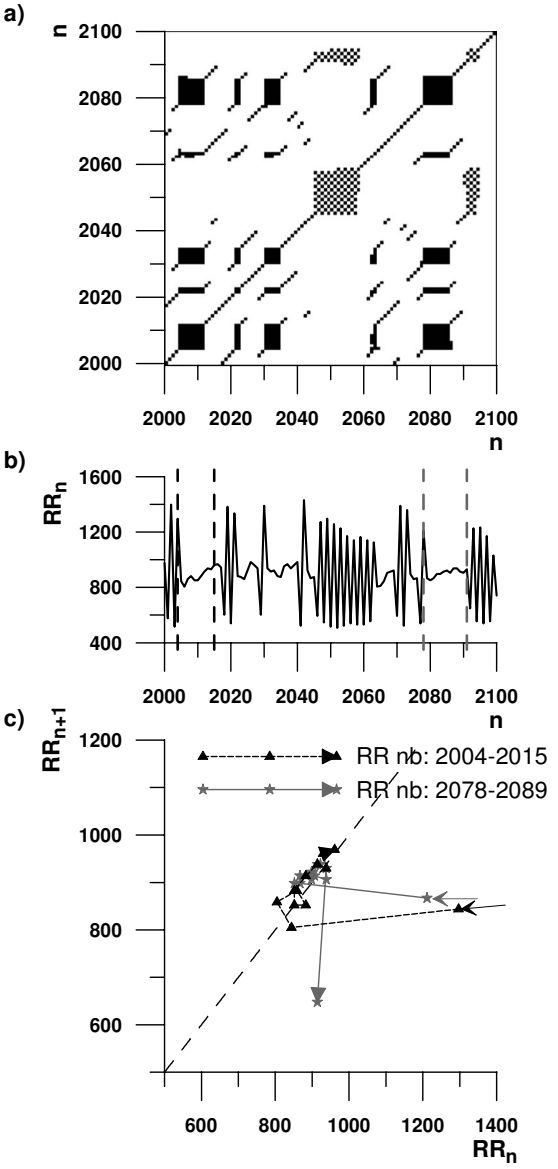

FIG. 27. (a) A fragment of the RP of the HRV data in Fig. 18—black squares are the signature of type I intermittency. (b) The raw data used to obtain (a). The detected laminar phases are marked by dashed lines. (c) The first return map for the selected parts of the HRV data in part (b)—two passages through a single intermittency channel are visible. The arrows depict the direction of motion.

IV. CONCLUSIONS

Recurrence plots can be used for detecting the effect of the proximity of the dynamical system to different types of bifurcation and the intermittencies which then occur. In this work, using both the generic models for the laminar phases, discrete models for complete intermittencies and also con-

tinuous time models for type II and type III intermittencies, we showed that by using recurrence plots it is possible to differentiate between all three Pomeau-Manneville intermittencies and to distinguish them from the chaos-chaos intermittency induced by an interior crisis.

When the examined time series is so short that the distribution of laminar phases may not be obtained due to poor statistics, the distinction between different kinds of intermittency may be made graphically. The RP patterns for laminar phases for Pomeau-Manneville intermittencies differ among themselves in the shape of the upper right corner. Type I intermittency forms uniformly black squares and rectangles, type II—a characteristic black kitelike shape, and type III—squares and rectangles with a rounded upper right corner inside a not fully darkened kitelike shape; for the crisis-induced chaos-chaos intermittency—black squares and rectangles dotted with a number of white points. The uniformly black bottom left corner of the shape characteristic for the laminar phase always has the shape of a square—it corresponds to the beginning of the laminar phase when the trajectory passes the immediate vicinity of the ghost of the fixed point. Then the location of the trajectory changes very slowly, so successive points of the trajectory are recurrent.

When the examined time series is long enough, the distribution of the parameter introduced in this paper—$\sqrt{F_a}$—can be obtained from the RP. These distributions are sufficiently similar to the distribution of the laminar phases characteristic for each of the different types of the intermittencies to allow distinguishing them. The effect of measurement noise complicates the distinction between the different kinds of intermittency but we were able to distinguish all the kinds of intermittency discussed here up to the level of 30% of measurement noise.

The method presented above was successfully applied to experimental data—heart rate variability recordings. The results obtained confirmed the results obtained earlier that type I intermittency is present in some cases of heart rate variability recordings.

The main advantage of the method presented in this paper is that it can be applied to short data series. Standard methods of distinguishing between different types of intermittencies require long time series. This method also allows us to detect a single passage of the trajectory through a laminar channel and also allows us to determine what type of intermittency this channel is related to. This means that having detected a single intermittent channel by its characteristic RP pattern we are able to state that the system is in the proximity of the bifurcation recognized in this way.

[1] E. Ott, *Chaos in Dynamical Systems* (Cambridge University Press, New York, 1993).
[2] Y. Pomeau and P. Manneville, Commun. Math. Phys. **74**, 189 (1980).
[3] H. G. Schuster, *Deterministic Chaos—An Introduction*, 2nd rev. ed. (VCH, Weinheim, 1988).
[4] T. J. Price and T. Mullin, Physica D **48**, 29 (1991).
[5] D.-R. He, D. Kai Wang, K.-J. Shi, C. Hai Yang, L. Yuan Chao, and J. Yue Zhang, Phys. Lett. A **136**, 363 (1989).
[6] M. Bauer, S. Habip, D. R. He, and W. Martienssen, Phys. Rev. Lett. **68**, 1625 (1992).
[7] N. Platt, E. A. Spiegel, and C. Tresser, Phys. Rev. Lett. **70**, 279 (1993).
[8] E. Covas, R. Tavakol, P. Ashwin, A. Tworkowski, and J. Brooke, Chaos **11**, 404 (2001).
[9] P. Ashwin, E. Covas, and R. Tavakol, Phys. Rev. E **64**, 066204 (2001).
[10] N. Marwan, N. Wessel, U. Meyerfeldt, A. Schirdewan, and J. Kurths, Phys. Rev. E **66**, 026702 (2002).
[11] N. Marwan and J. Kurths, Phys. Lett. A **336**, 349 (2005).
[12] J. P. Zbilut and C. L. Webber, Phys. Lett. A **171**, 199 (1992).
[13] J.-P. Eckmann, S. O. Kamphorst, and D. Ruelle, Europhys. Lett. **4**, 973 (1987).
[14] F. Takens, *Detecting Strange Attractors in Turbulence*, Dynamical Systems and Turbulence (Detecting Strange Attractors in Fluid Turbulence) Vol. 898 (Springer, Berlin, 1981), p. 366.
[15] L. Pecora, L. Moniz, J. Nichols, and T. Caroll, Chaos **17**, 013110 (2007).
[16] A. Albano, A. Mees, G. de Guzman, and P. Rapp, *Data Requirements for Reliable Estimation of Correlation Dimensions*, Chaos in Biological Systems (Plenum Press, New York, 1987).
[17] A. M. Fraser and H. L. Swinney, Phys. Rev. A **33**, 1134 (1986).
[18] C. J. Cellucci, A. M. Albano, and P. E. Rapp, Phys. Rev. E **71**, 066208 (2005).
[19] M. B. Kennel, R. Brown, and H. D. I. Abarbanel, Phys. Rev. A **45**, 3403 (1992).
[20] E. Kononov, http://www.myjavaserver.com/nonlinear/vra/download.html (2006).
[21] J. E. Hirsch, B. A. Huberman, and D. J. Scalapino, Phys. Rev. A **25**, 519 (1982).
[22] J.-Y. Huang and J.-J. Kim, Phys. Rev. A **36**, 1495 (1987).
[23] P. Richetti, F. Argoul, and A. Arneodo, Phys. Rev. A **34**, 726 (1986).
[24] A. Nayfeh and B. Balachandran, *Applied Nonlinear Dynamics* (John Wiley and Sons, Inc., New York, 1995).
[25] J. Żebrowski, Acta Phys. Pol. B **32**, 1531 (2001).
[26] J. J. Żebrowski and R. Baranowski, Physica A **336**, 74 (2004).
[27] J. M. Gac and J. J. Żebrowski, Phys. Rev. E **73**, 066203 (2006).